LANGMUIR

Article

pubs.acs.org/Langmuir

Simulated Permeation and Characterization of PEGylated Gold Nanoparticles in a Lipid Bilayer System

Priyanka A. Oroskar,[†] Cynthia J. Jameson,[†,‡] and Sohail Murad*[,†,§]

[†]Department of Chemical Engineering, University of Illinois at Chicago, 810 South Clinton Street, Chicago, Illinois 60607, United States

[‡]Department of Chemistry, University of Illinois at Chicago, 845 West Taylor Street, Chicago, Illinois 60607, United States

[§]Department of Chemical and Biological Engineering, Illinois Institute of Technology, 3300 South Federal Street, Chicago, Illinois 60616, United States

Supporting Information

ABSTRACT: PEGylated gold nanoparticles are considered suitable nanocarriers for use in biomedical applications and targeted drug delivery systems. In our previous investigation with the alkanethiol-functionalized gold nanoparticle, we found that permeation across a protein-free phospholipid membrane resulted in damaging effects of lipid displacement and water and ion leakage. In the present study, we carry out a series of coarse-grained molecular simulations to explore permeation of lipid bilayer systems by a PEGylated gold nanoparticle, especially at the bulk-liquid−lipid interface as well as the interface between the two lipid leaflets. Initially, we examine molecular-level details of a PEGylated gold nanoparticle (constructed from cycled annealing) in water and find a distribution of ligand configurations (from mushroom to brush states) present in nanoparticles with medium to high surface coverage. We also find that the characteristic properties of the PEGylated gold nanoparticle do not change when it is placed in a salt solution. In our permeation studies, we investigate events of water and ion penetration as well as lipid translocation while varying the ligand length, nanoparticle surface coverage, and ion concentration gradient of our system. Results from our studies show the following: (1) The number of water molecules in the interior of the membrane during ligand-coated nanoparticle permeation increases with PEG*n*-SH surface coverage, ligand length, and permeation velocity but is not sensitive to the ion concentration gradient. (2) Lipid molecules do not leave the membrane; instead they complete trans-bilayer lipid flip-flop with longer ligands and higher surface coverages. (3) The lack of formation of stable water pores prevents ion translocation. (4) The PEGylated nanoparticle causes less damage to the membrane overall due to favorable interactions with the lipid headgroups which may explain why experimentalists observe endocytosis of PEGylated nanocarriers in vivo.

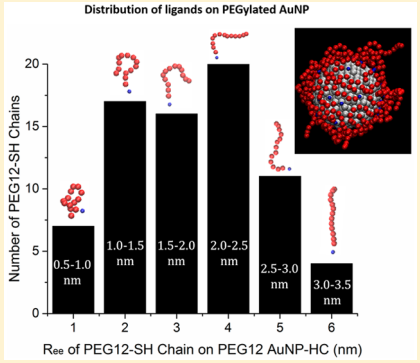

1. INTRODUCTION

In targeted drug delivery systems, nanoparticle carriers are often functionalized with polyethylene glycol (PEG) polymers to improve solubility and in vivo stability in biological media.[1−3] Gold nanoparticles decorated with ligands are desirable candidates in particular for delivery of therapeutic agents due to their distinctive physical and chemical characteristics, which include the ability to be synthesized in a wide range of shapes and the ease of functionalization of the nanoparticle surface.[4,5] In this study, we have carried out a series of coarse-grained molecular dynamics simulations to investigate the effect of permeation of a polyethylene-glycol-functionalized gold spherical nanoparticle across a protein-free phospholipid bilayer membrane with special attention given to the barriers to permeation at the bulk-liquid−lipid interfaces. Investigation of permeation effects of functionalized nanoparticles under various conditions is important because it can guide in developing nanoparticle carriers with minimized cytotoxic effects as they permeate cell membranes in vivo. Our previous work focused on understanding the effect of ligand length on alkanethiol-functionalized nanoparticle permeation of membranes; presently we are concentrating our efforts on ligands such as PEG that are being used widely in biomedical drug delivery applications. For instance, the circulation time of nanoparticles in the blood has been found to increase due to PEGylation,[6] which has prompted studies such as interaction of PEG with erythrocytes.[7] Upon intravenous administration of PEGylated nanoparticles in the blood, erythrocytes are likely the first cells to come in contact with the functionalized nanocarrier.[7] Therefore, it is important to evaluate the effect PEGylated nanoparticles have on lipid membranes (also present in erythrocytes) since damage to erythrocytes may result in in vivo cytotoxicity.

Previously we have shown that ligand-coated gold nanoparticle permeation across lipid bilayer membranes induces water and ion penetration, as well as incidence of lipid flip-flop

Received: May 6, 2016
Revised: June 30, 2016
Published: July 11, 2016

DOI: 10.1021/acs.langmuir.6b01740
Langmuir 2016, 32, 7541−7555

and repeated instances of lipid displacement; here we report on these types of events induced by permeation of spherical gold nanoparticles protected with a known biocompatible functional group (PEG*n*-SH). In this work, we compare the results of permeation by a gold nanoparticle functionalized with PEG*n*-SH ligands to our previous work with alkanethiol-coated gold nanoparticles. Our former studies serve as a benchmark to understand ligand-coated nanoparticle permeation and support this current study of a nanoparticle functionalized with material used frequently in drug delivery applications. We vary the system ion concentration gradient, length of grafted PEG ligands, and chain density of grafted ligands to observe the effect on water and ion leakage, lipid flip-flop, and lipid loss from the lipid bilayer membrane. In our previous studies with an alkanethiol-functionalized gold nanoparticle, we observed that the number of water molecules found in the lipid membrane interior increases with ligand length, nanoparticle size, and permeation velocity but is not sensitive to ion concentration gradient. In those studies, formation of water fingers as a mechanism of ion translocation across the membrane was examined in addition to displacement of lipid molecules that do not complete the flip-flop. These effects of ligand-coated nanoparticle permeation are detrimental to the cellular environment and can result in apoptosis. In the present work, in addition to the aforementioned permeation effects, the mechanism of penetration of the PEG-functionalized spherical nanoparticles especially into the water−bilayer interface and subsequently at the interface between the two lipid leaflets and the nature of the interactions between the PEG ligands and the lipids of the bilayer are closely examined. The results of this study should facilitate the work of experimentalists who engineer nanoparticles with biocompatible surface modifications for biomedical applications.

2. METHODS

2.1. Coarse-Grained Model. In carrying out our molecular dynamics simulations, we have used a coarse-grained model of a DPPC lipid bilayer membrane as our model phospholipid bilayer membrane[8] and a coarse-grained model of PEG in our functionalized gold nanoparticle.[9] Our gold nanoparticle core is treated as a rigid body while the PEG ligands are flexible and move freely during the permeation. In coarse-grained models, small clusters of atoms are treated as interaction sites. This grouping of atoms reduces the degrees of freedom in a system but allows the simulation to be more efficient at extending time scales compared to atomistic simulations. Coarse-grained methods for molecular dynamics simulations have been employed frequently to study large biomolecular systems. Previously, many groups have studied the behavior of PEG molecules in water based and other systems using molecular dynamics.[10−12] In our study, we use the MARTINI force field developed by Marrink and co-workers[13] which has been verified to accurately reproduce semi-quantitatively the fundamental thermodynamic and structural properties of proteins, amino acids, and lipid bilayer membranes.[14] Our present system includes both nonbonded and bonded as well as charged interaction sites, all represented with different interaction parameters particular to the type of interaction site. The MARTINI force field contains pretested interaction parameters for polar (P-type), nonpolar (N-type), apolar (C-type), and charged (Q-type) interaction sites. Nonbonded interactions between particle−particle pairs are characterized by a shifted Lennard-Jones (LJ) potential energy function where

$$U_{\mathrm{LJ}}(r_{ij}) = 4\epsilon_{ij}[(\sigma_{ij}/r_{ij})^{12} - (\sigma_{ij}/r_{ij})^{6}] \tag{1}$$

r_{ij} represents the distance between the interacting particle pairs and ε_{ij} is the depth of the LJ potential well. In the MARTINI model, most interacting particle pairs have an effective distance of σ_{ij} = 0.47 nm; however, for charged- or apolar-type interaction sites, the effective distance of σ_{ij} = 0.62 nm is applied. The depth of the well, ε_{ij}, is a parameter specific to the interacting particle pairs and varies from ε_{ij} = 2.0 to 3.1 kJ/mol for polar and nonpolar site types and to represent interactions with charged particles in apolar environments. ε_{ij} ranges from 3.5 to 5.6 kJ/mol for interaction sites that are strongly polar or nonpolar such as in aliphatic chains.

The shifted Coulombic potential energy function, which is used to model interactions between charged particle types, is described by

$$U_{\mathrm{el}}(r) = \frac{q_i q_j}{4\pi\epsilon_0\epsilon_r r} \tag{2}$$

The weak harmonic potential energy function used to model interactions between bonded particle pairs is represented in the MARTINI force field by

$$V_{\mathrm{bond}}(R) = \frac{1}{2}K_{\mathrm{bond}}(R - R_{\mathrm{bond}})^2 \tag{3}$$

where the equilibrium distance R_{bond} is 0.47 nm. The force constant, K_{bond}, is 1250 kJ/(mol nm^2). In systems where bonded interacting pairs have complex chemical structures, bond angles must be accounted for by the MARTINI force field to more accurately represent the bond configuration. For this, a weak harmonic potential of the cosine type, $V_{\mathrm{angle}}(\theta)$, is employed, where

$$V_{\mathrm{angle}}(\theta) = \frac{1}{2}K_{\mathrm{angle}}[\cos(\theta) - \cos(\theta_0)]^2 \tag{4}$$

In addition to bond and angle configurations, dihedral interactions between quadruplets of atoms in PEG are accounted for in the MARTINI force field by a dihedral potential, where

$$V_{\mathrm{dihedral}}(\varphi) = \sum_{i=1}^{m} K_{\varphi,i}[1 + \cos(n_i\varphi + \varphi_i)] \tag{5}$$

In the original coarse-grained model of PEG and PEO,[15] a force constant of 85 kJ/mol was used with an angle potential of the cosine type (eq 4). Later it was determined that numerical stability improved when a force constant of 50 kJ/mol was used with an angle potential of the harmonic type where

$$V_{\mathrm{angle}}(\theta) = K_{\mathrm{angle}}[\theta - \theta_0]^2 \tag{6}$$

Rather than eq 4, we use eq 6 with the new parameters from the most recent paper by Lee and Pastor[16] to validate our modification against the original MARTINI model. Two critical parameters for polymers are the radius of gyration, R_g, and root-mean-square end-to-end distance ($\langle R_{ee}\rangle$). In the original MARTINI model, the R_g and $\langle R_{ee}\rangle$ values found for PEG9 in water were 6.3 ± 0.1 and 15.7 ± 0.1 Å, respectively. In these simulations, a single PEG9 chain was placed in a box of size 10.0 × 10.0 × 10.0 nm^3 containing ∼9200 previously equilibrated coarse-grained water molecules and simulated for 400 ns at 296 K with pressure maintained at 1 bar using the *NPT* ensemble time integrator. The results for R_g and $\langle R_{ee}\rangle$ were obtained from four simulations of different starting points for the PEG9 chain with data from the first 20 ns omitted. Repeating these simulations with the updated parameters for our adopted model resulted in R_g and $\langle R_{ee}\rangle$ of 6.4 ± 0.03 Å and 14.69 ± 0.17 Å, respectively, in reasonable agreement with the original coarse-grained model. We note that we use a methyl-terminated form of PEG*n* (sometimes referred to as PEO*n*) which has "*n* + 1" coarse-grained beads as described by the MARTINI model.

2.2. Cycled Annealing of PEG*n*-SH onto a Bare Gold Nanoparticle. As in our previous studies, the 3.0 nm diameter gold nanoparticle is obtained by cutting a nearly spherical structure from a bulk face-centered-cubic (FCC) lattice of gold atoms. To condense the PEG*n*-SH ligands onto the surface of the nanoparticle, a cycled annealing simulation procedure was used, as in studies of nanoparticles immersed in polymer melts, for example, polymer nanocomposites or polystyrene or poly(ethylene oxide) doped with nanoparticles or nanorods.[17−21]

DOI: 10.1021/acs.langmuir.6b01740
Langmuir 2016, 32, 7541−7555

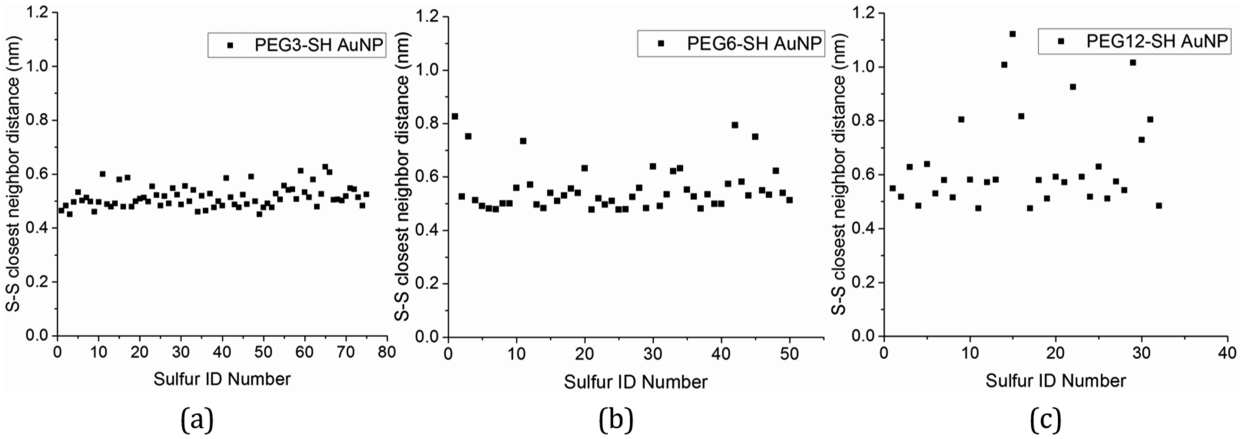

Figure 1. Distance between neighboring sulfur atoms on (a) PEG3-SH-AuNP, (b) PEG6-SH-AuNP, and (c) PEG12-SH-AuNP obtained from cycled annealing simulations.

We start by equilibrating a 10.0 × 10.0 × 10.0 nm^3 simulation box of PEG3-SH and obtained a density of 1053.6 kg/m^3 using the *NPT* ensemble time integrator at 400 K (above the glass transition temperature of PEG[22]) for 5 ns. This is close to the value 1048 kg/m^3 from experimental measurement and extrapolation.[20,23] Into this we inserted a 3.1 nm diameter gold nanoparticle in an *NVE* ensemble at 400 K for another 5 ns. After equilibration, we switched to the *NPT* ensemble time integrator for the cycled annealing simulation. In all of our cycled annealing simulations, the thiol group is the attachment site of the PEG*n*-SH ligand. The temperature was cycled from 300 to 1100 K to allow the ligands to explore various stable binding sites on the nanoparticle and to permit any excess ligands to desorb from the nanoparticle surface. Temperatures of up to 1200 K have been used for silica nanoparticles[24] with PEG polymer chains. During the cooling stages of the annealing procedure, we allowed the temperature to drop by 20 K/ns for 5 ns. Once this was completed, the system was equilibrated for 50 ns at 400 K and finally for 50 ns at 323 K, the temperature used in our permeation simulations.

In our previous work, we used the cycled annealing procedure to condense butanethiol ligands onto the nanoparticle surface and then replaced these short ligands with alkanethiol ligands of desired length.[25] In constructing PEG*n*-SH-functionalized gold nanoparticles for simulations with various ligand lengths, it is not accurate to assume that coverage is independent of ligand length, since it has been found in experimentally synthesized PEGylated nanoparticles that the coverage density of PEG on the nanoparticle surface does decrease as the chain length or molecular weight increases.[26] This is consistent with experimental work by Rahme et al.[28] where it was observed that the grafting density of the mPEG-SH ligands on a gold nanoparticle 15 nm in diameter decreased from 3.93 to 0.31 $PEGnm^{-2}$ as the molecular weight of the ligands increased from 2100 to 51400 g mol^{-1}, respectively, which the authors attribute to increased steric hindrance and polymer conformational entropy with an increase in the PEG chain length.

For the cycled annealing simulation with PEG3-SH ligands, 75 ligands were found to condense on the nanoparticle surface (shown in Figure 1a) which is equivalent to a coverage of 2.49 ligands/nm^2. Since our desired PEGylated nanoparticles for study are PEG6-SH-AuNP and PEG12-SH-AuNP, we used our equilibrated PEG3-SH-AuNP nanoparticle in solution of PEG3-SH ligands as a starting point for our next simulations. We attached additional beads to the condensed ligands to match the ligands in the melt to mimic a PEG6-SH- and PEG12-SH-AuNP in solution of their respective melts. The nanoparticle with the longer ligands was then equilibrated in its solution and then subjected to the same cycled annealing simulation we employed for PEG3-SH-AuNP. We obtained a PEG6-SH-AuNP with 50 ligands condensed and a PEG12-SH-AuNP with 32 ligands condensed, equivalent to a coverage of 1.66 and 1.06 ligands/nm^2, respectively. Many groups[27] who synthesized PEGylated nanoparticles reported a range in PEG coverage from 0.2 to 2.0 ligands/nm^2 with the exception of Rahme et al.,[28] who observed a higher grafting density of 3.93 ligands/nm^2, which indicates that our constructed PEG*n*-SH nanoparticle in simulation has grafting densities in accordance with what is found experimentally.

In order to observe differences in membrane interaction with a nanoparticle of higher coverage, we did test a PEG6-SH- and PEG12-SH-AuNP with a coverage of 2.49 ligands/nm^2 by adding beads to the structure obtained from cycled annealing with PEG3-SH, without further annealing.

For the remainder of the discussions in this work, we will be referring to the PEG12-SH-AuNP with lower coverage of 1.06 ligands/nm^2 and the one with coverage of 2.49 ligands/nm^2 as PEG12-AuNP-LC and PEG12-AuNP-HC, respectively. The same naming convention will be used for the nanoparticles functionalized with PEG6-SH ligands, PEG6-AuNP-LC for the nanoparticle with coverage of 1.66 ligands/nm^2 and PEG6 AuNP-HC for the nanoparticle with coverage of 2.49 ligands/nm^2.

3. CHARACTERIZATION OF THE PEGYLATED AUNP

3.1. PEGylated Gold Nanoparticle in Water. After cycled annealing, we introduce the equilibrated nanoparticle into a simulation box with previously equilibrated water molecules by removing all water molecules that would have overlapped with the nanoparticle. After equilibration in aqueous solution for 200 ns, we obtained the characteristics of PEG6-AuNP-HC, PEG6-AuNP-LC, PEG12-AuNP-HC, and PEG12-AuNP-LC, shown in Tables S1−S4, namely, the average radius of the functionalized nanoparticle, average volume occupied by an attached chain, average radius of gyration (R_g), and average end-to-end distance of individual grafted chains ($\langle R_{ee} \rangle$). All these properties are strongly dependent on the nature of the interface between the ligands and the bulk-liquid phases, and by investigating these properties we have attempted to better understand these interfaces as well. The average radius of the functionalized nanoparticle is defined as the mean distance between the center of the gold core and the terminal bead of the grafted ligands. The average volume of a single attached PEG*n*-SH chain is obtained by calculating the volume difference of the gold nanoparticle pre- and postfunctionalization and dividing this by the number of grafted PEG*n*-SH chains. This method is the same as that reported by Li et al.[29] in their computational analysis of a PEGylated nanoparticle with varying coverage densities. In addition, we have studied the behavior of the PEG*n*-AuNP-LC and PEG*n*-AuNP-HC nanoparticles in a salt solution in preparation for conducting

DOI: 10.1021/acs.langmuir.6b01740
Langmuir 2016, 32, 7541−7555

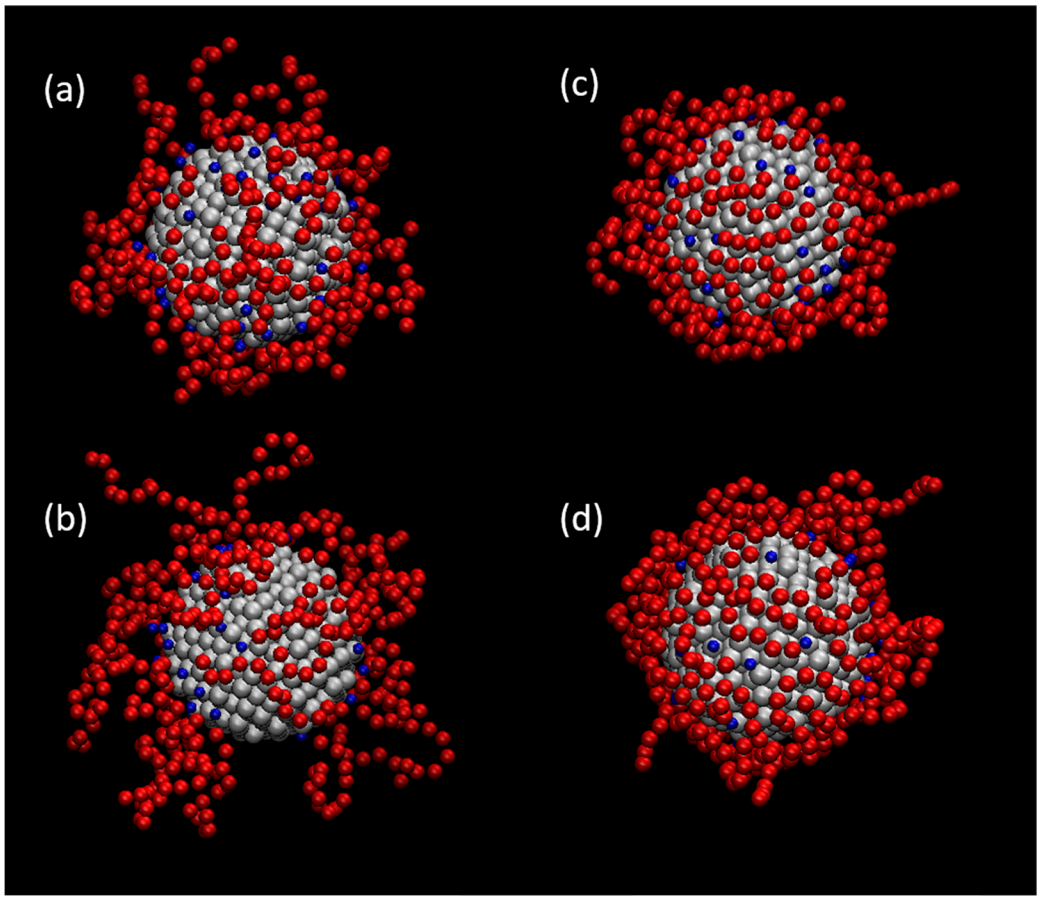

Figure 2. Snapshots of equilibrated PEG6-AuNP-LC (a, c) and PEG12-AuNP-LC (b, d) in the melt state (a, b) and in water (c, d). The gold nanoparticle core is pictured in white with the sulfur beads (blue) and PEG*n* ligands (red). For clarity, the solvent molecules are not shown.

permeation studies for systems under an ion concentration gradient. After 200 ns of equilibration, we obtained the same set of characteristics to compare the behavior of the nanoparticle in water and in a salt solution. Each value in Tables S1−S4 was collected by averaging configurations of the PEGylated AuNP every 100 ps over 1 ns after 200 ns of equilibration in solution was completed.

3.2. Characteristics of the Nanoparticle in Polymer Melt vs in Water. From Tables S1 and S3 (Supporting Information (SI)), it is clear that the radius of gyration and average radius of the functionalized nanoparticle decrease in water compared to that in the polymer melt. In comparing data in Tables S1 and S2 of the SI and also in Tables S3 and S4 of the SI, it is clear that the radius of gyration and average radius of the functionalized nanoparticle increases with increasing surface coverage density. The average volume per PEG*n*-SH ligand also decreases for both the PEG6-AuNP-LC and PEG12-AuNP-LC when the functionalized nanoparticles are equilibrated in water compared to the polymer melt. For both the PEG6-AuNP-LC and PEG12-AuNP-LC, the average R_g do not differ significantly for the nanoparticle in the melt and in water. For the PEG6-AuNP-LC and PEG12-AuNP-LC in water, the $\langle R_{ee} \rangle$ is larger for the nanoparticle in the melt than in water. The standard deviation of the average R_g is small compared to that of the $\langle R_{ee} \rangle$ for the nanoparticles in the melt and in water and salt solutions. As indicated in Tables S1−S4 of the SI, there is a slight increase in average volume of individual PEG*n*-SH chains as surface coverage density increases for both the PEG6-SH and PEG12-SH cases; the difference is not significant however. The $\langle R_{ee} \rangle$ of individual PEG12-SH ligands increases as coverage density increases (as seen in Tables S3 and S4 of the SI) but does not show significant difference between PEO6-AuNP-LC and -HC (as seen in Tables S1 and S2 of the SI). In observing the differences between the nanoparticles equilibrated in water and salt solution from Tables S1−S4 of the SI, we find that the average radius of the functionalized nanoparticle and average R_g and $\langle R_{ee} \rangle$ of the individual chains are all within one standard deviation of another.

In order to have a clearer understanding of what types of molecular configurations correspond to these averages (and differences in the observed behavior), we examine the snapshots in Figure 2 to observe the configurations of ligands on a typical PEGylated AuNP in the polymer melt and after equilibration in water. In Figure 2, we present snapshots of the PEGylated nanoparticles in the melt state (Figure 2a,b) and after equilibration in water (Figure 2c,d). These snapshots represent a typical PEGylated nanoparticle, while the data in Tables S1−S4 of the SI are averages over 1 ns after equilibration is complete.

In the melt, the PEG*n*-SH polymers that condensed on the nanoparticle surface are seen to be stretched out and interacting with other polymers in the melt (surrounding the PEGylated AuNP, but not explicitly shown in Figure 2). On the other hand, panels c and d of Figure 2 show that, in the presence of water, the PEG6-SH and PEG12-SH chains are collapsed or wound in loops close to the nanoparticle surface, and the chains are in a more coiled form as opposed to stretched out and flattened as in the melt. More attractive intermolecular

DOI: 10.1021/acs.langmuir.6b01740
Langmuir 2016, 32, 7541−7555

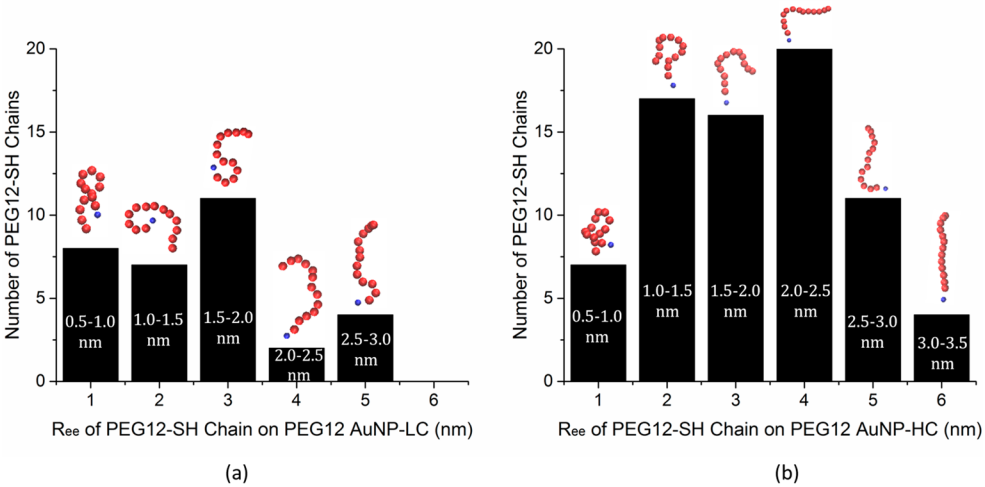

Figure 3. Distribution of R_{ee} of ligands on (a) PEG12-AuNP-LC and (b) PEG12-AuNP-HC equilibrated in water. Snapshots of typical PEG12-SH from that distribution are included with blue representing the thiol atom and red the beads of PEG12. These are averages over 1 ns after equilibration is complete.

interactions between PEG*n*-SH polymers cause them to stretch out in the melt state to interact with the surrounding polymers and to coil closer together in the presence of water molecules. As seen in Figure 1b,c, in the melt, the longer ligands are found not as evenly distributed onto the surface as were the shortest ligands. This is most likely due to the attached ligands that are collapsed or curled up close to the surface of the nanoparticle (shown in snapshots in Figure 2a,b) which can block surrounding ligands from adsorbing onto the surface during the annealing process. The distance between neighboring sulfur atoms increases with the length of the ligand in the melt due to the fact that longer ligands will cover a larger area of the nanoparticle surface when collapsed. As expected from experimental findings,[28] we find that the surface coverage decreases as the ligand length in the melt increases. The decrease of average radius and R_g of the PEGylated AuNP in the melt state compared to that in water is a result of PEG*n*-SH polymers being more attracted to each other than they are to water, leading them to entangle around each other and the nanoparticle surface. The entanglement and coiling of the polymers is clearly shown in our snapshots (Figure 2) providing a molecular view of PEG ligands in the melt and PEG ligands in water. The decreased average V_{ligand} in water for both the PEO12-SH-AuNP and PEO6-SH-AuNP compared to the melt is consistent with the molecular view in Figure 2 where the PEG*n*-SH ligands collapse or coil close to the nanoparticle surface, resulting in a loss of conformational degrees of freedom for each grafted chain. The molecular view of the PEGylated AuNP in the melt state in Figure 2 is consistent with the larger volume per ligand and higher conformational degrees of freedom of ligands in the stretched state. PEG*n*-SH chains that have larger values of average R_g and $\langle R_{ee} \rangle$ are stretched away from the nanoparticle surface and are in a flattened form. This indicates that, in the polymer melt, PEG*n*-SH polymers are stretched further away from the gold nanoparticle surface (shown in Figure 2). The small standard deviation of the R_g of individual PEG chains on the PEGylated AuNP in the melt and after equilibration in water therefore suggests that R_g does not give a suitable description of how the PEG*n*-SH chains are behaving. Essentially, the average R_g of an individual PEG chain does not describes whether the ligand is stretched out or coiled close to the surface of the nanoparticle, only the overall space it is contained in.

3.3. Distribution of Ligand Configurations in a PEGylated AuNP. As already observed in the snapshots of Figure 2, ligands are not uniformly coiled or stretched out but rather have a distribution of molecular configurations and a distribution of individual $\langle R_{ee} \rangle$ values. For the $\langle R_{ee} \rangle$ of individual chains, the larger standard deviations in Tables S1−S4 of the SI imply that there is a wider distribution of configurations exhibited by the attached ligands, from the curled-up to the stretched state. Therefore, in Figure 3 we further examine the distribution of $\langle R_{ee} \rangle$ values that are found on the PEG12-AuNP for both coverages. In Figure 3, we also quantify the distribution of various ligand configurations present on the equilibrated PEG12-AuNP. Above each bar, we provide a molecular-level view of a typical configuration of the PEG12-AuNP-LC and PEG12-AuNP-HC ligands equilibrated in water. In the bar graphs of Figure 3, we find that there is a wide distribution of $\langle R_{ee} \rangle$ values for individual ligands in both low and high coverage cases, with a broader distribution for the high coverage situation.

We observe from the snapshots of typical ligand configurations corresponding to each bar of $\langle R_{ee} \rangle$ values that there are an array of ligand configurations that the PEG12-SH ligand can take, ranging from the coiled to the stretched state. This indicates that on a typical PEGylated nanoparticle, there are many configurations of ligands from mushroom-type (smaller $< R_{ee} >$) to brush-type (larger $\langle R_{ee} \rangle$) conformations. This behavior is once again strongly dependent on the interface between the ligands and the water/polymer melt phases. The "mushroom" description corresponds to a distribution of largely coiled and more flat-lying molecular configurations, although there exists a small fraction of extended ligands even in the case of the PEG12-AuNP-LC. The "brush" description corresponds to a large fraction of molecular ligand configurations that are stretched, although a fraction of coiled ligands are present even for the PEGylated AuNP at higher coverages.

Several groups that have studied PEGylated nanoparticles in water or in polymer melt observe the behavior of PEG in the so-called "mushroom" or "brush" regimes, both theoretically and experimentally, depending on coverage, the so-called grafting density.[30−34] Within the mushroom regime where

DOI: 10.1021/acs.langmuir.6b01740
Langmuir 2016, 32, 7541−7555

coverage density is low, PEG chains tend to collapse on the surface of the nanoparticle. In the case of low grafting density, the volume of a single PEG chain is large due to more conformational degrees of freedom. In the case of high grafting density, or the brush regime, it has been observed that the PEG chains tend to be stretched away from the nanoparticle surface, a reasonable mechanism for minimizing steric repulsions and system free energy. This results in a significant loss of conformational degrees of freedom for the PEG chain, which leads to a small available volume per PEG polymer. From our results we find that the transition from mushroom to brush behavior of individual PEG ligands would occur gradually as the surface coverage density increases, as the distributions depicted in Figure 3 would change from panel a to panel b. Tables S1 and S2 of the SI indicate that the $\langle R_{ee} \rangle$ does not change significantly as the coverage density increases on the PEO6-AuNP. This further demonstrates that the transition between mushroom to brush regimes is not sharp and that high grafting densities will not result in a brush only regime; there is always a distribution present, and it is illustrated best when comparing nanoparticles with coverage densities that largely differ from one another, as in Figure 3.

It has been observed, both in simulation and experiment, that the average volume of individual PEG polymers grafted to nanoparticles ranging from 8.0 to 90.0 nm in diameter decreases nonlinearly as grafting density increases.[29,35] This is a result of the transition of PEG polymers from the mushroom to the brush configuration where PEG polymers begin to compact with neighboring chains. In smaller nanoparticles such as the one used in the current study (3.1 nm in diameter), increased surface curvature leads to reduced steric contacts between grafted polymers[17,36] and average volume of PEG polymers is larger for smaller nanoparticles with the same coverage density as those with larger core diameter. For this reason, we believe we do not observe a significant difference in average volume occupied by PEG*n*-SH polymers with increasing coverage density when comparing with our smaller nanoparticle.

The behavior of PEG had been observed to change in the presence of salt, and this has been ascribed to the strong association of sodium ions to PEG.[37,38] Others have observed (in all-atom simulations) a single PEG chain wrapping around sodium ions and forming helical-like structures[39,40]. The characteristic properties of the PEGylated AuNP equilibrated in salt solution in Tables S1−S4 of the SI did not deviate from those in water, which indicates that the overall structure of the functionalized nanoparticle does not change significantly from equilibration in pure water. We believe this is due to competition between the PEG*n*-SH chains and the sodium ions present in solution. The situation where a single PEG chain is in a salt solution[37] is quite different since the sodium ions have only one chain to interact with. Where multiple chains are present, sodium ions have multiple atoms to interact with and may not associate with one chain in particular. In addition, in cases of nanoparticles functionalized with polymers, there is a tendency for chains to collapse and form loops close to the nanoparticle surface (as observed in Figure 2), and this leaves few grafted chains the opportunity to interact with ions in the surrounding solution.

4. PEGYLATED AUNP PERMEATION IN DPPC LIPID BILAYER MEMBRANES

The simulation system (Figure 4) is 12.8 × 12.6 × 30.0 nm^3 in size and consists of a dipalmitoylphosphatidylcholine (DPPC)

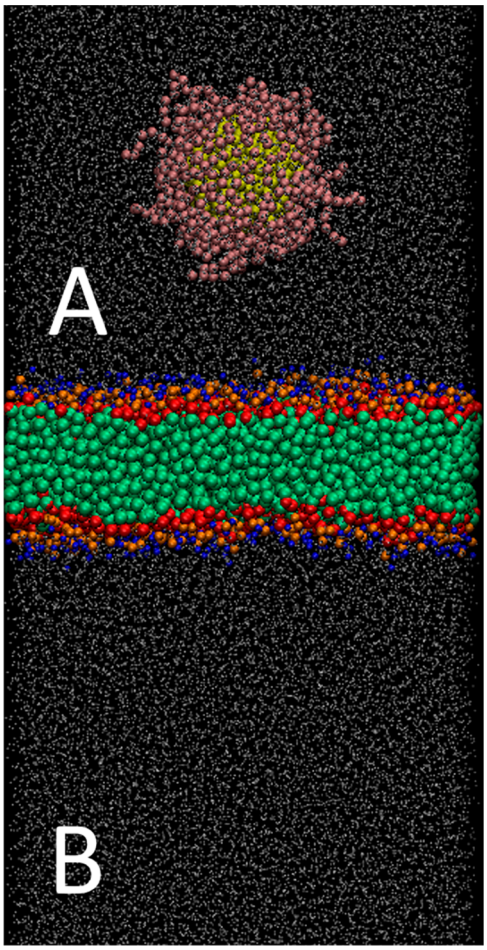

Figure 4. DPPC lipid bilayer membrane simulation system for investigation of PEGylated nanoparticle permeation from the top compartment (A) to the bottom compartment (B) across the lipid bilayer membrane (blue = choline, orange = phosphate, red = glycerol, green = lipid tails, white = water, gold = nanoparticle core, and pink = PEG*n*-SH ligands).

membrane with 512 DPPC molecules and approximately 33,600 CG water molecules. We have observed in previous studies that this lipid membrane self-assembles from an isotropic solution of DPPC lipid molecules and water in a coarse-grained simulation.[41] We have found that the properties of this self-assembled DPPC lipid bilayer are in good agreement with experimental measurements, which validates the efficacy of the model[42] and its ability to correctly represent the interface between the lipid and water as well as the interface between the two lipid leaflets. In experiments investigating lipid membrane permeation, phospholipid molecules are maintained on solid supports such as polymers[43] that mimic the role of the extracellular membrane matrix in vivo. In order to replicate actual permeation experiments closely in our molecular simulation, we tethered roughly 8% of the boundary lipid molecules (1 nm from the edge of the membrane) to their initial position using a harmonic spring force. Tethering ensures that the entire membrane does not translate during simulated

DOI: 10.1021/acs.langmuir.6b01740
Langmuir 2016, 32, 7541−7555

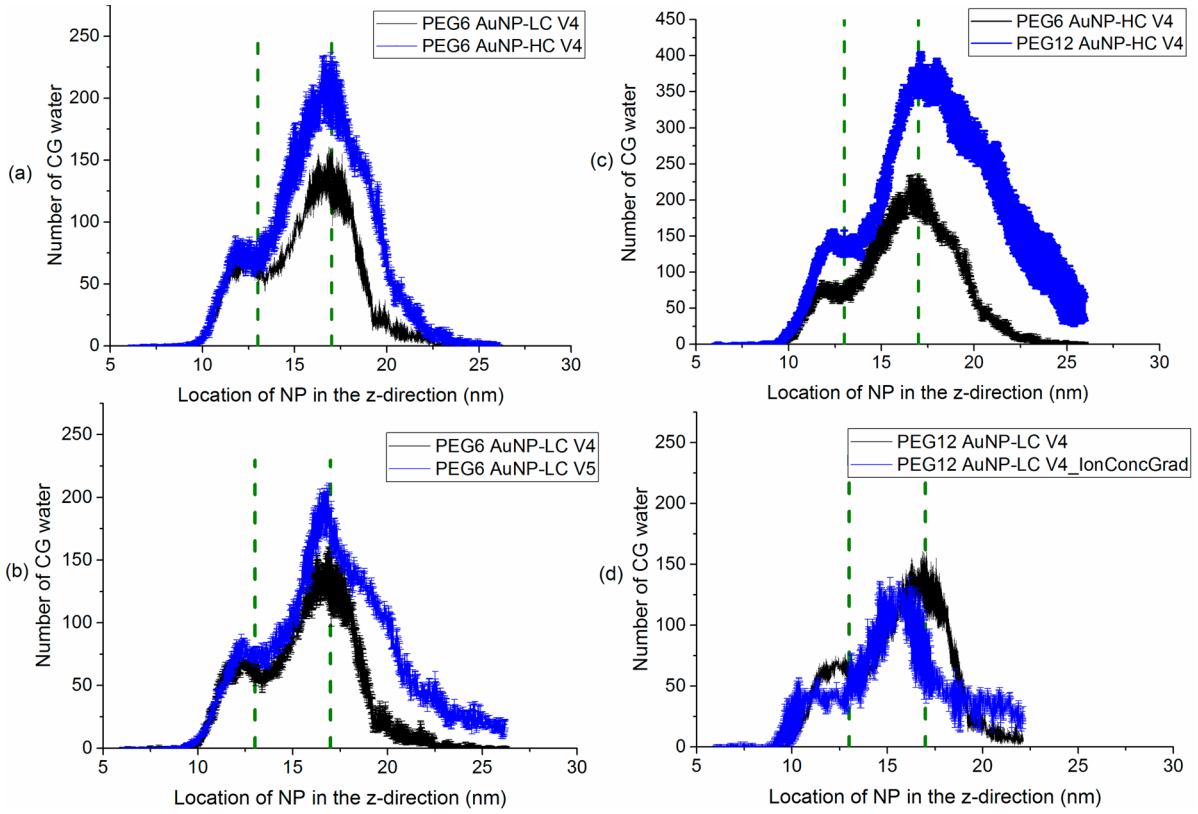

Figure 5. Number of coarse-grained water molecules that permeate into the hydrophobic membrane interior during PEGylated gold nanoparticle permeation under the following conditions: (a) Effect of coverage density, (b) effect of nanoparticle velocity, (c) effect of PEG length, and (d) effect of ion concentration gradient. The green dashed lines represent the equilibrated position of the phosphate groups in the top and bottom leaflets of the DPPC lipid bilayer membrane. Each data point has error bars included based on three independent simulations.

nanoparticle permeation. A PEGylated gold nanoparticle will translocate from compartment A to compartment B (in Figure 4) across the lipid membrane under constant velocity, effectively representing an experimental test where a functionalized nanoparticle transporting from the extracellular (compartment A) to the intracellular space (compartment B). All PEGylated NP permeation simulations were performed using the LAMMPS[44] molecular dynamics simulation package where a Langevin thermostat was employed to maintain the system temperature at 323 K. An *NVE* ensemble time integrator and periodic boundary conditions were also applied to our system that utilized a time step of 10 fs to ensure membrane stability during the simulation.

For our simulations, we used gold nanoparticles that are 3.0 nm in diameter. In previous studies using alkanethiol-functionalized gold nanoparticles with gold cores of 2.0 and 3.0 nm in diameter, we found that most significant results on lipid flip-flop, ion leakage, and lipid displacement occur with the larger nanoparticle.[45] Therefore, in the present study, we solely focused on the larger gold nanoparticle (3.0 nm in diameter). For practical applications, much larger nanoparticles, 10−100 nm in diameter, are readily carried in vivo in circulating blood.[46,47] The parameters varied in this work include nanoparticle velocity, ligand length (PEG6-SH and PEG12-SH each with 8 and 14 CG beads, respectively), and ion concentration gradient. For systems with unequal ion concentrations, sodium and chloride ions were added to the top compartment A of the system (Figure 4) at 1.4 mol % concentration (under the saturation limit, 1.8 mol % of sodium chloride in water). As in our previous work,[42] the system under unequal ion concentration gradient also contained two walls (cut from an FCC structure and placed on either side of the system in Figure 4) that are impermeable to water and ions, to isolate the ions in the top compartment (compartment A) which would otherwise move to the bottom compartment due to the periodic boundary conditions.

In our work, complete membrane recovery is achieved when zero water molecules are found in the membrane interior. This is often accomplished by allowing the system to continue to equilibrate once the nanoparticle permeation has completed; for systems such as the current one where low velocities are used, full membrane recovery often occurs when the nanoparticle has reached the end of the simulation box.

We found in earlier studies with our alkanethiol-functionalized LCNP that the larger nanoparticles and longer ligands caused more damage to the lipid bilayer membrane and increased the recovery time after permeation. Lower velocities allow the functionalized nanoparticle to sample multiple configurations and increases interaction time with surrounding particles as it moves through the system. Since our current study involves nanoparticles with even longer ligands than used in our previous work, the nanoparticle velocities tested in this study (PEG6-SH-AuNP were 0.05, 0.075, 0.1, and 0.2 m/s; for the PEG12-SH-AuNP they were 0.025, 0.05, 0.075, and 0.1 m/s) are lower than in our previous work (0.35−1.0 m/s). We will refer to velocities 0.025, 0.05, 0.075, 0.1, and 0.2 m/s as V1, V2, V3, V4, and V5, respectively. The velocities tested in this study are comparable to actual cases where PEGylated nanoparticles are injected into the body; for example, Bishop et al. previously

DOI: 10.1021/acs.langmuir.6b01740
Langmuir 2016, 32, 7541−7555

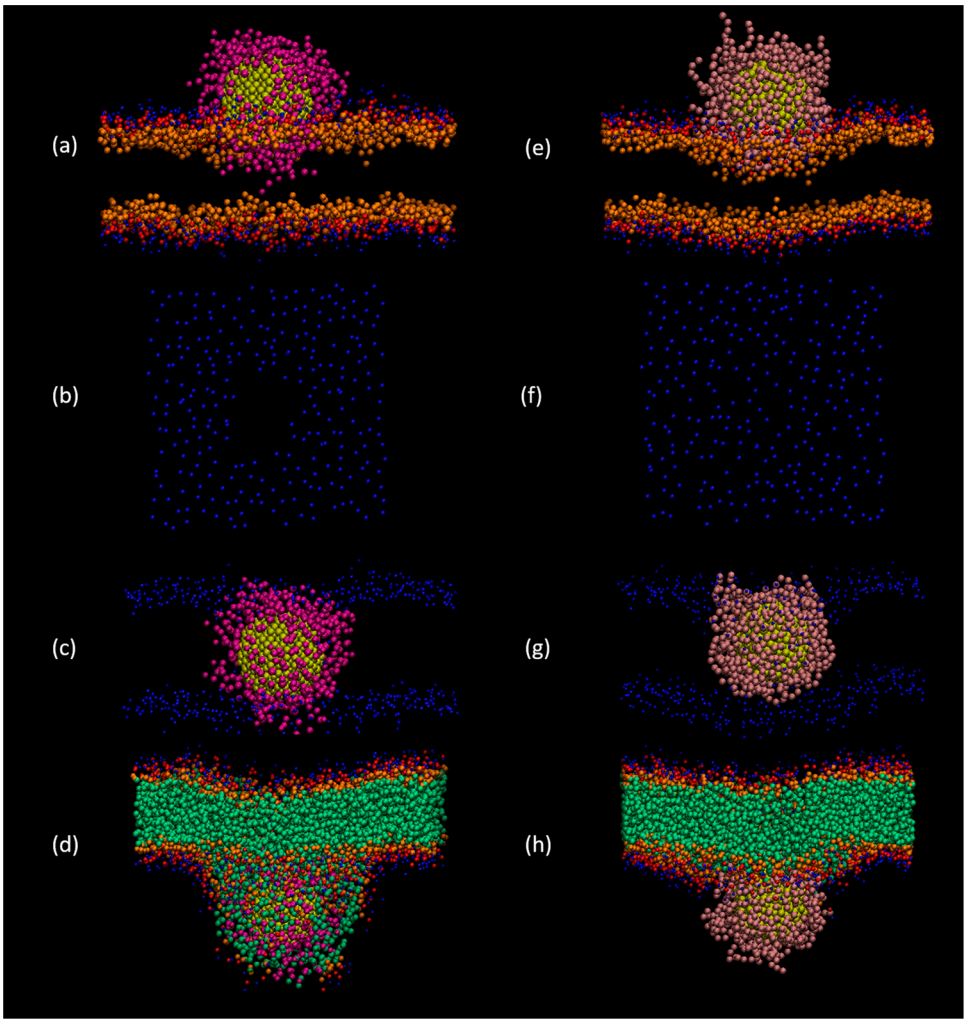

Figure 6. Snapshots of the (a, b, c, d) alkanethiol-coated gold nanoparticle and (e, f, g, h) PEG6-AuNP-HC. Snapshots indicate (a, e) the approach of the nanoparticle to the top leaflet of the membrane, (b, f) top view of the choline headgroups of the first membrane leaflet, (c, g) nanoparticle located in the middle of the membrane, and (d, h) nanoparticle leaving the bottom leaflet of the membrane. Each set of snapshots contains omitted atoms (blue = choline, red = phosphate, orange = glycerol, green = alkyl tails, yellow = gold nanoparticle, pink = PEG6-SH ligands, and magenta = alkanethiol ligands).

measured the typical blood flow velocity in the middle cerebral artery to range from 0.36 to 1.4 m/s.[48]

5. RESULTS AND DISCUSSION

5.1. Water Penetration. In the present study, we examined water penetration as a result of nanoparticle permeation and investigated its dependence on permeation velocity, ion concentration gradient, and PEG*n*-SH ligand length and ligand coverage density. We compare and contrast this to the water penetration data we obtained in our previous study with alkanethiol-coated nanoparticles. From our previous work and those of other investigators, nanocarriers permeating from the extracellular to intracellular space are known to induce defects and pore formation in the membrane which facilitates water leakage into the hydrophobic membrane interior.[49,50] In this study, as in our previous studies, water penetration is defined as the number of coarse-grained water molecules, originally present in the top compartment of the lipid bilayer membrane, that are found to have moved into the membrane by nanoparticle permeation. The hydrophobic interior of the lipid membrane is the region extending 0.75 nm in both the $+z$ and $-z$ directions from the center of the lipid bilayer membrane. This includes the lipid bilayer tail region in the membrane at equilibrium. The water molecules positioned at the phosphate heads at the entrance region of the formed water pore are not counted in the total number of waters leaking into the membrane interior.

We now report, in Figure 5a–d, our observations on water leakage due to PEGylated nanoparticle permeation under varying conditions of nanoparticle velocity, surface coverage, ligand length, and ion concentration gradient. In each case, we have quantified the number of water molecules entering into the hydrophobic membrane interior throughout the course of the nanoparticle permeation. Water penetration can occur from both the top and bottom membrane compartments. In Figure 5a–d, the green dotted lines represent equilibrated positions of the phosphate groups in the DPPC lipid head in the top and bottom membrane leaflets, which represents the location of the lipid–water interface.

We observe some similarities and differences in the water penetration behavior for the PEG*n*-AuNP-HC and -LC nanocarriers compared to alkanethiol-functionalized nanoparticles that may be attributed to the different chemical behavior of the ligands during interaction with water, ions, and

DOI: 10.1021/acs.langmuir.6b01740
Langmuir 2016, 32, 7541–7555

the lipid bilayer molecules. One major distinction of the water leakage behavior is how water molecules behave when the nanoparticle core is inside the membrane. It is clear from Figure 5a–d that when the core of the PEG*n*-AuNP is inside the membrane interior, water molecules are still entering the membrane along with the nanoparticle. In examining water leakage profiles from our previous study, we observed that the number of water molecules moving into the hydrophobic membrane interior decreases as the NP core reaches the inside of the membrane. This initial decrease is in part due to the space occupied by the LCNP, leaving little room for water molecules to penetrate the membrane interior, and also the unfavorable interaction between the alkyl ligands and water in the hydrophobic environment which causes some water molecules to be readily expelled. In the present case of the PEO*n*-AuNP, our findings that water penetration does not decrease as the PEO*n*-AuNP reaches inside the membrane interior can be attributed to the favorable interaction of water with the PEO*n* ligands permitting water molecules to be carried along with the nanoparticle into the membrane interior.

As seen in Figure 5a, the number of water molecules permeating the hydrophobic membrane interior increases with increasing nanoparticle ligand length. We had previously observed that longer ligands induce more disturbances to the membrane integrity and result in formation of larger water pores.[45] This increases the recovery time of the membrane and allows water molecules to continue permeating into the membrane interior.

In Figure 5b, we observe the number of water molecules penetrating the hydrophobic membrane interior to increase with increasing nanoparticle permeation velocity as the nanoparticle exits the second leaflet of the membrane (the second lipid–water interface) into compartment B of Figure 4. Initially, the number of water molecules penetrating the membrane is relatively insensitive to changing velocities; however, later during the permeation higher nanoparticle velocities induce more disruption to the lipid membrane, and this results in the development of a larger water pore. With higher velocities, the lipid membrane takes more time to recover after the permeation cycle is complete and, as a consequence, more water molecules continue to penetrate the membrane as the nanoparticle completes the permeation. As found previously, this effect is greatest for nanoparticles with longer length ligands; in the current study, the same behavior is observed.

We have also examined the effect of nanoparticle surface coverage density on water penetration in lipid membranes. It is observed in Figure 5c that water penetration increases with increasing coverage density. Increasing the number of surface ligands increases the average radius and R_g of the functionalized nanoparticle, as shown in Tables S1–S4. Essentially, a nanoparticle with more surface ligands corresponds to a larger effective size of nanoparticle. This introduces a larger water pore in the membrane during permeation, which in turn allows more water molecules to reach the membrane interior.

It is clear from Figure 5d that the number of water molecules penetrating does not differ significantly when an ion concentration gradient is introduced. We observed this as well in our previous work with the bare and alkanethiol-coated gold nanoparticles. Since chemical potential driving force in our system is very weak (compartment A contains a 1.4 mol % solution of NaCl), we do not expect water penetration to be sensitive to an ion concentration gradient.

5.2. Nanoparticle Penetration into a Bilayer. In our previous work we observed few lipid flip-flop events to occur with alkanethiol-coated nanoparticle permeation; instead a majority of the lipid molecules that were displaced from the top layer of the membrane during permeation were dislodged and carried into the bulk solution entangled in the ligands of the nanoparticle. We found that this occurred due to the lipid molecule associating closely with a specific group of ligands on the alkanethiol-coated nanoparticle arising from the favorable hydrophobic interaction occurring between the lipid tails and alkanethiol ligands. In the present study, we observe very few such lipid displacement events as a result of PEO*n*-AuNP permeation.

In Figure 6 we display snapshots of the PEO6-AuNP-HC permeation in contrast to the alkanethiol-coated gold nanoparticle (3.1 nm in diameter, R_g = 1.70 nm, close to the size of the PEO6-AuNP-HC, R_g = 1.76 nm) both with velocity of 0.2 m/s. Snapshots from Figure 6a,e were taken when the average position of the nanoparticle was 1.0 nm above the equilibrium position of the phosphate groups from the top bilayer membrane leaflet (when the nanoparticle has partially penetrated the lipid–water interface). The top views of the choline groups in the first membrane leaflet at the same position of the nanoparticle in Figure 6a,e are shown in Figure 6b,f. In Figure 6c,g, the snapshot displayed is when the average position of the functionalized nanoparticle is in the center of the membrane, halfway between the equilibrated positions of the phosphate groups in the top and bottom membrane leaflets. For Figure 6d,h, snapshots were taken when the average position of the nanoparticle was 2.0 nm away from the equilibrium position of the phosphate groups in the bottom leaflet of the bilayer membrane (it exits as the second lipid–water interface). We chose to display these snapshots to give a distinct picture of how the permeation differs between the PEO*n*ylated nanoparticle and alkanethiol-coated nanoparticle from our previous studies.

When the alkanethiol-coated gold nanoparticle approaches the top leaflet of the bilayer membrane (the lipid–water interface), it breaks through the lipid headgroups (as shown in Figure 6a) and disturbs the integrity of the membrane which changes the nature of the ligand–water interface and its ability to resist penetration of "foreign molecules". The headgroups of DPPC do not have a favorable interaction with the alkanethiol ligands, so they are pushed away from the nanoparticle when it is penetrating the first membrane leaflet. This differs from the approach of the PEG6-AuNP-HC to the top membrane leaflet (Figure 6e) where lipid membrane develops a curvature while still maintaining its integrity (continuous lipid–water interface) and continuity as a leaflet. In examining the top view of the first leaflet of the bilayer membrane in Figure 6b,f, it is clear that the alkanethiol ligands have completely pushed the lipid headgroups apart to create a hole in the membrane, in contrast to the PEG ligands which do not break the lipid membrane headgroups apart but, instead, curve upward toward the other ligands and nanoparticle core. This is a possible explanation as to why many experimentalists observe the receptor-mediated endocytosis of PEGylated nanoparticles and wrapping of lipid membranes around them.[51,52] In our system, we cannot observe wrapping of the membrane because we are employing a system that is tethered at the edges. The observance of membrane curving instead of breaking indicates that lipid membranes are able to wrap around PEGylated nanoparticles more easily than alkanethiol-coated gold nanoparticles because

DOI: 10.1021/acs.langmuir.6b01740
Langmuir 2016, 32, 7541–7555

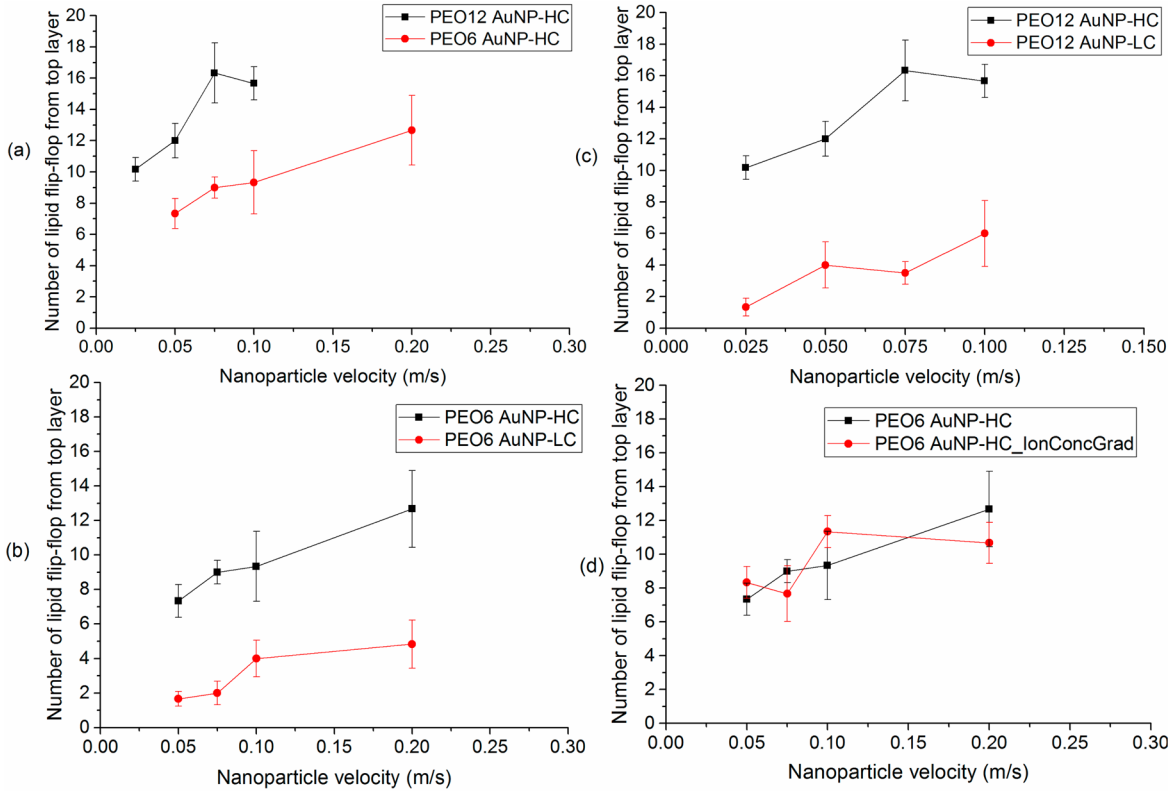

Figure 7. Number of lipid flip-flop events that occur during PEGylated gold nanoparticle permeation under the following conditions: (a) Effect of ligand length, (b, c) Effect of coverage density, (d) Effect of ion concentration gradient. Each data point has error bars included based on three independent simulations.

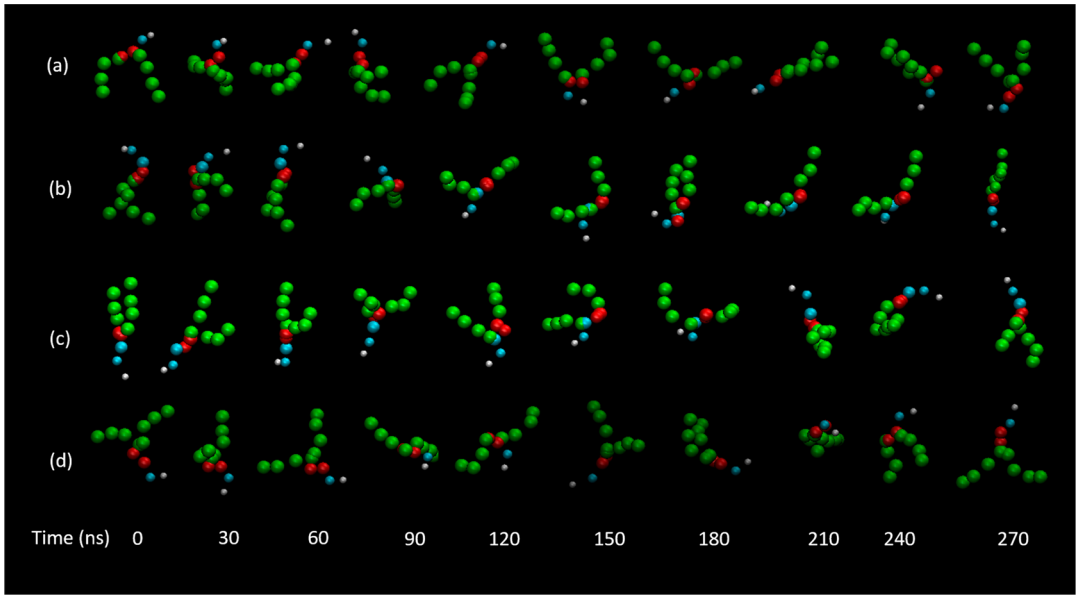

Figure 8. Snapshots of lipid flip-flop events from the top leaflet (a, b) and bottom leaflet (c, d) of the membrane with a PEG12-AuNP-HC with permeation velocity of 0.075 m/s.

of the favorable interaction between the PEG ligands and lipid headgroups. In any in vivo condition, the endocytosis of nanoparticles is receptor-mediated where receptors enhance the cellular uptake of the PEGylated nanoparticle. Even without receptors present in the present study, we can reason that endocytosis may be feasible since the PEG ligands do not break through the membrane.

Snapshots from Figure 6c,g show the difference in behavior of ligands when the functionalized nanoparticle is in the middle of the top and bottom membrane leaflets (the interface between the two lipid leaflets). The ligands of the alkanethiol-functionalized nanoparticle (Figure 6c) continue to be stretched and interact with the lipid tails in the surrounding environment. The ligands of the PEGylated nanoparticle

DOI: 10.1021/acs.langmuir.6b01740
Langmuir 2016, 32, 7541−7555

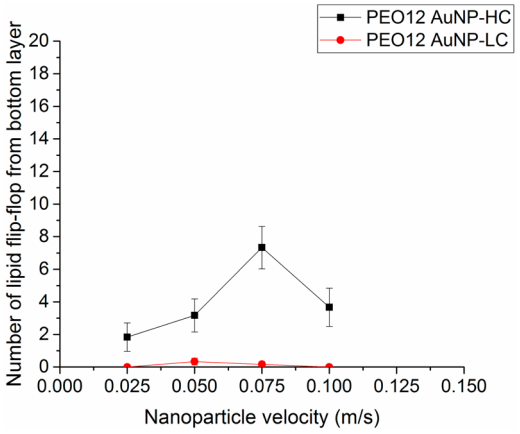

Figure 9. Effect of surface coverage on the number of lipid molecules to flip-flop from the bottom membrane leaflet. Error bars are based on three independent simulations.

(Figure 6g), in contrast, are not stretched out, indicating a less favorable interaction with the lipid tails of the membrane. Also, the snapshot shows the PEG ligands near the top leaflet of the membrane to be stretched out and interacting with DPPC headgroups; this further emphasizes the favorable interaction of the PEG ligands with the choline, phosphate, and glycerol headgroups.

It is clear that as the alkanethiol-coated nanoparticle (Figure 6d) is leaving the second membrane leaflet (the second lipid–water interface), DPPC molecules are surrounding the nanoparticle due to the favorable interaction between the lipid tails and alkanethiol ligands. In contrast, observation of the PEG6-AuNP-HC leaving the second membrane leaflet (Figure 6h) shows that lipid molecules are not dragged by the nanoparticle upon exit from the membrane. As a result, very few lipid molecules have an opportunity to be displaced from the membrane because of the less favorable interaction of the alkyl tails and the hydrophilic PEG6-SH chain.

5.3. Lipid Flip-Flop. Lipid flip-flop events occur when a lipid molecule translocates from one leaflet of a bilayer membrane to the other leaflet across a pore or defects in the lipid bilayer, thus changing the nature of the lipid–water interfaces; defects are induced by nanocarrier permeation as we have shown in previous studies.[45] This biological process is usually supported by lipid translocators such as integral and transmembrane proteins or specific enzymes known as flippases that can catalyze lipid flip-flop[53]. It has been observed experimentally that certain peptides can accelerate the rate of lipid flip-flop through membrane pores comprised of peptides and lipid molecules[54]. Natural lipid membranes are asymmetric and unnecessary lipid flip-flop events can affect the process of molecule recognition at the outer bilayer surface; this in turn can have detrimental effects on cell lifetime.[55]

In Figure 7, we observe that the number of lipid flop–flop events increases with longer ligand lengths and with increased surface coverage density for all conditions. Longer ligands disturb the membrane integrity more during the permeation, and this results in more lipid molecules being dislocated from the top layer of the membrane, thereby permitting the lipid molecules to complete a flip-flop. For nanoparticles with increased surface coverage density, there are more ligands to disturb the top layer of the membrane, and therefore, larger numbers of lipid molecules are flipped. We do not observe sensitivity to ion concentration gradient in the number of lipid flip-flop events, for reasons mentioned earlier.

In Figure 8, we show snapshots of typical lipid flip-flop events that take lipid molecules from the top membrane leaflet to the bottom membrane leaflet (Figure 8a,b) and from the bottom membrane leaflet to the top membrane leaflet (Figure 8c,d). Our snapshots indicate that in both cases of lipid flip-flop from the top or bottom leaflet of the membrane, we observe the same mechanism to occur; the lipid molecule undergoes a full reorientation in the *z*-direction through the pore formed by the PEGylated nanoparticle and joins the opposite membrane leaflet. We have not observed this particular phenomenon previously in our studies with bare or alkanethiol-coated gold nanoparticles. Only a few lipid molecules flip-flop from the bottom membrane leaflet for nanoparticle permeation with the shorter PEG6-AuNP, at any coverage. The combination of longer ligand length and increased coverage density (PEG12-AuNP-HC) results in greater incidences of lipid flip-flop from the bottom membrane leaflet (as shown in Figure 9). Gold nanoparticles with long ligands such as PEG12-SH cause larger

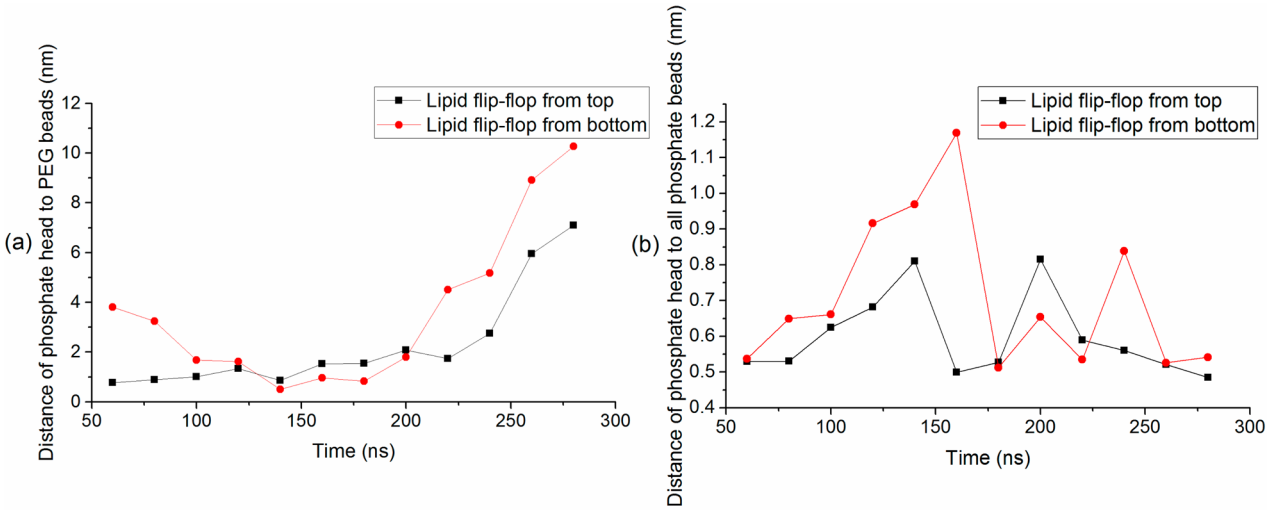

Figure 10. Distance from phosphate headgroup of lipid molecule that translocated to the opposite membrane leaflet to (a) PEG beads in the PEG12-AuNP-HC and (b) other phosphate groups in the top and bottom leaflets of the membrane (at permeation velocity of 0.075 m/s).

DOI: 10.1021/acs.langmuir.6b01740
Langmuir 2016, 32, 7541–7555

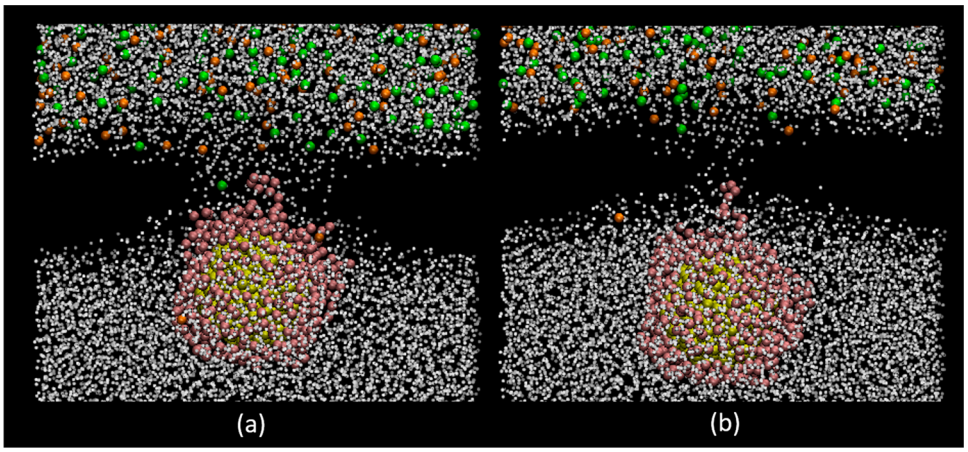

Figure 11. Snapshots of water column formation when (a) water penetration is at a maximum and (b) when the nanoparticle is leaving the bottom leaflet of the membrane. This system contains an ion concentration gradient system with PEG12-AuNP-LC permeating at a velocity of 0.075 m/s (white = water, orange = sodium, green = chloride, pink = PEG12-SH, and yellow = gold nanoparticle).

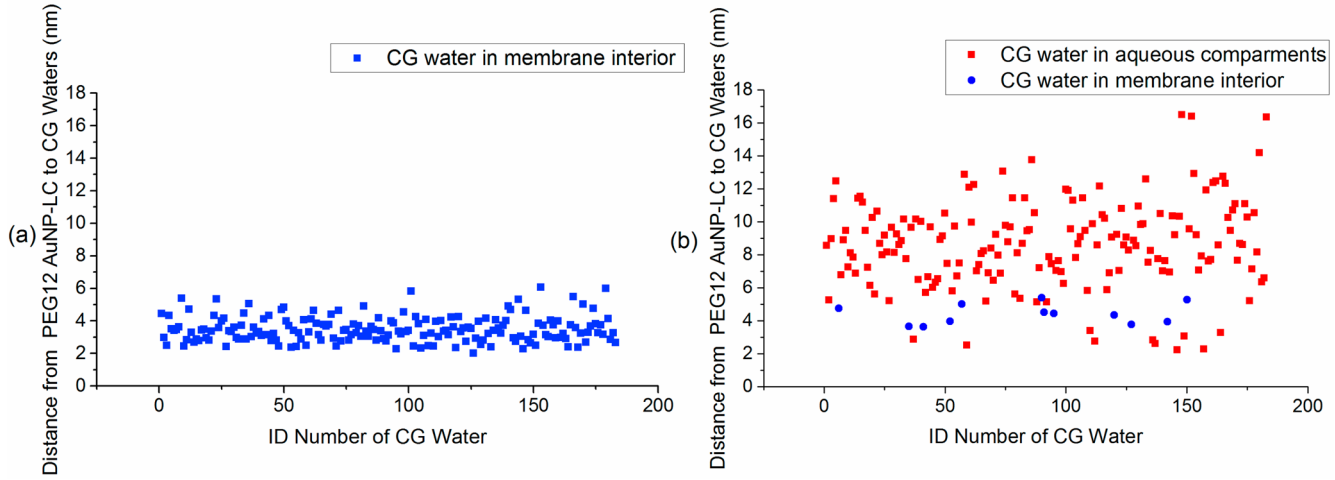

Figure 12. Distance from center of PEG12-AuNP-LC to CG water molecules found in the hydrophobic membrane interior when (a) water penetration is at a maximum and (b) distance to the same CG water molecules when the nanoparticle is leaving the bottom leaflet of the membrane.

perturbations to the lipid membrane system during permeation and cause lipid molecules from the bottom leaflet to be displaced at the time when the nanoparticle penetrates the top leaflet of the membrane. In Figure 10a, we show the distance between the phosphate head of a lipid molecule and PEG beads in the functionalized nanoparticle and in Figure 10b, the distance between the phosphate head of the flip-flopping molecule and surrounding phosphate groups. We see in Figure 10a that for a lipid molecule flip-flopping from the top leaflet, the PEG beads will interact with the phosphate head (or lipid molecule) until it has completed its flip-flop at around 225 ns where it moves away from the lipid molecule along with the nanoparticle as it continues its permeation. For a lipid molecule flip-flopping from the bottom leaflet, we see in Figure 10a that the phosphate headgroup does not interact with the PEG beads until they approach the second leaflet (about 150 ns). In Figure 10b we see clearly for both a lipid molecule flip-flopping from the top and bottom, the favorable hydrophilic interaction between the lipid headgroups allows the phosphate heads to remain close to one another even after the lipid head of the flip-flopping molecule moves toward the PEG beads in the nanoparticle. This causes the lipid flip-flop to complete as opposed to the lipid molecule leaving the membrane to the bulk solution along with the nanoparticle.

In biological systems, lipid molecules naturally flip-flop between bilayer membrane leaflets.[56] For experimental cases of asymmetrical membranes then, the delivery of PEGylated nanoparticles can cause unnecessary lipid exchange to take place between bilayer membrane leaflets; this would change the identity of the membrane, and it may hamper important biological processes. Synthesized gold nanoparticles functionalized with PEG for drug delivery contain PEG chains with large molecular weights (~2000 Da in some cases which indicates a PEG chain with roughly ~44 units).[57,58] Our results suggest that in actual experimental studies where long PEG chains protecting nanoparticles are delivered in vivo, transbilayer lipid flip-flop may occur that could damage the cell.

5.4. Minimal Translocation of Ions with Nanoparticle Permeation. Ion permeation across lipid bilayer membranes occurs when ions translocate from the extracellular to intracellular cell space via pore-mediated or other forms of assisted transport.[59] As we have observed, nanoparticle permeation induces a water pore in the lipid membrane through which water molecules can travel from one compartment to another. In the present study, we carried out

DOI: 10.1021/acs.langmuir.6b01740
Langmuir 2016, 32, 7541−7555

permeation simulations of our system under an ion concentration gradient to observe whether ions also penetrate through the induced hydrophilic pore.

The ions in our system present in the aqueous solution of compartment A of Figure 4 cannot permeate the lipid membrane unaided because of the resistance offered at the lipid−water interface to such permeation, owing to their Columbic interaction with the phospholipid headgroups. The highly hydrophobic interior (especially the interface regions between the two lipid leaflets) of the lipid membrane also prevents ions from permeating and restricts them to the aqueous solution and phospholipid headgroups. We observed in our previous work with the bare gold nanoparticle that most ions that enter the water pore return to the bulk solution although there are a few that travel along water columns or "fingers" that form between both membrane compartments and span the lipid membrane. In situations where an alkanethiol-coated gold nanoparticle with long ligands was used, it was found that water finger formation was absent and therefore ion transport events were few to none. For the present study, we conducted a large number of nanoparticle permeation simulations with the PEGylated gold nanoparticle and examined 48 independent simulations for systems under an ion concentration gradient to observe water finger formation and whether PEG-SH ligands affected ion transport across the lipid membrane.

We found that ion penetration events were sensitive to nanoparticles with longer ligands and higher coverage; in both cases a larger water pore is formed which allows more ions to cross the lipid membrane. We did not find any sensitivity to nanoparticle velocity.

In Figure 11 we display snapshots of the water column formed during PEG12-AuNP-LC nanoparticle permeation when the number of water molecules in the hydrophobic membrane interior have reached a maximum (Figure 11a) and when the nanoparticle is 2.0 nm away from the equilibrated position of the phosphate groups in the bottom leaflet of the lipid membrane. In Figure 11b we observe the rapid loss of the water column. We show in Figure 12a the distance between the PEG12-AuNP-LC and the water molecules found in the membrane interior and in Figure 12b the distance between the same water molecules and the functionalized nanoparticle when it is located 2.0 nm away from the phosphate groups in the bottom leaflet. As the nanoparticle leaves the second leaflet of the bilayer membrane, the water finger quickly collapses; water molecules and ions return to the aqueous water compartment. This is shown in Figure 12 where it is clear that the water molecules (colored in red) found in the membrane interior have moved far from the nanoparticle and returned to the top or bottom compartment as the nanoparticle continues to permeate the membrane. This short-lived water column allows for very few ions to permeate the lipid membrane. It is also apparent from our examination of water penetration that as soon as the nanoparticle crosses the second membrane leaflet, the lipid membrane begins to recover and water molecules return to the bulk solution. Furthermore, our snapshots from Figure 6d,h also show that even though PEG-SH ligands may be entangled in the phospholipid head-groups as the nanoparticle crosses the second membrane leaflet, the overall disturbance to the membrane is minimal since the lipid molecules are not dragged by the nanoparticle and the membrane is allowed to recover immediately after permeation. This then drives ions to return to the interfacial and phospholipid headgroup region

Overall, more chloride ions penetrate the membrane compared to sodium ions. In our previous work we found that sodium ions concentrate near the phospholipid headgroups while chloride ions have a tendency to stay close to the interfacial region (found in other studies as well).[42,59] The lower surface charge density of the chloride ion increases the flexibility of the hydrated ion, which allows it to easily integrate itself in water networks formed across water pores in lipid membranes induced by nanoparticle permeation. This agrees with our findings that more chloride ions translocate across the lipid membrane by integrating themselves into water fingers through interaction with surrounding water molecules. However, the number of these ion transport events are small in comparison to the number of ions present in the bulk solution (∼1000 sodium and chloride ions); a maximum of five chloride ions and three sodium ions were found to have penetrated the membrane with the PEG12-AuNP-HC.

6. CONCLUSION

In this work, we have explored the effect of PEGylated gold nanoparticle permeation on a model DPPC lipid bilayer membrane to investigate the water penetration, ion translocation, and lipid flip-flop events that take place which may lead to cell cytotoxicity and often negative implications for nanocarriers used in drug delivery applications. Our simulated experiments represent practical applications of drug delivery methods where PEGylated nanocarriers are sometimes used in various biomedical applications. We examined characteristic properties and molecular-level details of ligands on PEGylated gold nanoparticles with varying ligand lengths and surface coverages. Special attention was paid to the behavior at the lipid−bulk-liquid interface at the entry point, the interface between the two lipid leaflets, and the lipid−liquid interface at the exit point. We showed that the so-called mushroom and brush descriptions that have been applied to PEGylated AuNPs at low and high surface coverage limits actually correspond to a continuous shift in distribution of ligand configurations from a large fraction of coiled to a large fraction of stretched, but a distribution of configurations persist at all coverages. In contrast to the alkanethiol-coated gold nanoparticle used in our previous studies, the PEGylated gold nanoparticle permeation appeared significantly less harmful to the integrity of the membrane because it did not result in loss of lipids from the membrane. Even in the case of the longer PEG*n*-SH ligands and higher surface coverages used in this study, the induced water penetration, ion transport, and lipid flip-flop are minimal. The results of this study, which highlight effects of using a hydrophilic ligand, should be of some aid to experimentalists who are designing nanocarriers for biomedical applications. Molecular-level dynamics information provided by our simulations gives strong indication that nanocarriers with PEGylated surfaces may be considered desirable candidates for drug delivery applications.

■ ASSOCIATED CONTENT

Supporting Information

The Supporting Information is available free of charge on the ACS Publications website at DOI: 10.1021/acs.langmuir.6b01740.

DOI: 10.1021/acs.langmuir.6b01740
Langmuir 2016, 32, 7541−7555

Characteristic properties of individual PEG ligands on PEGylated nanoparticles simulated after cycled annealing and equilibration in water (PDF)

AUTHOR INFORMATION

Corresponding Author

*E-mail: murad@iit.edu. Phone: (312)- 567-3867.

Notes

The authors declare no competing financial interest.

ACKNOWLEDGMENTS

This research has been funded by a grant from the National Science Foundation (Grant No. CBET-0730026/1263107)

REFERENCES

(1) Pissuwan, D.; Niidome, T.; Cortie, M. B. The forthcoming applications of gold nanoparticles in drug and gene delivery systems. *J. Controlled Release* **2011**, *149* (1), 65−71.

(2) Ghosh, P.; Han, G.; De, M.; Kim, C. K.; Rotello, V. M. Gold nanoparticles in delivery applications. *Adv. Drug Delivery Rev.* **2008**, *60* (11), 1307−1315.

(3) Soppimath, K. S.; Aminabhavi, T. M.; Kulkarni, A. R.; Rudzinski, W. E. Biodegradable polymeric nanoparticles as drug delivery devices. *J. Controlled Release* **2001**, *70* (1), 1−20.

(4) Mout, R.; Moyano, D. F.; Rana, S.; Rotello, V. M. Surface functionalization of nanoparticles for nanomedicine. *Chem. Soc. Rev.* **2012**, *41* (7), 2539−2544.

(5) Cao, Y.; Zheng, R.; Ji, X.; Liu, H.; Xie, R.; Yang, W. Syntheses and Characterization of Nearly Monodispersed, Size-Tunable Silver Nanoparticles over a Wide Size Range of 7−200 nm by Tannic Acid Reduction. *Langmuir* **2014**, *30* (13), 3876−3882.

(6) Yoo, J. W.; Chambers, E.; Mitragotri, S. Factors that control the circulation time of nanoparticles in blood: challenges, solutions and future prospects. *Curr. Pharm. Des.* **2010**, *16* (21), 2298−2307.

(7) He, Z.; Liu, J.; Du, L. The unexpected effect of PEGylated gold nanoparticles on the primary function of erythrocytes. *Nanoscale* **2014**, *6* (15), 9017−9024.

(8) Yuan, H.; Jameson, C. J.; Murad, S. Diffusion of gases across lipid membranes with OmpA channel: a molecular dynamics study. *Mol. Phys.* **2010**, *108* (12), 1569−1581.

(9) Song, B.; Yuan, H.; Jameson, C. J.; Murad, S. Permeation of nanocrystals across lipid membranes. *Mol. Phys.* **2011**, *109* (11), 1511−1526.

(10) Choi, E.; Mondal, J.; Yethiraj, A. Coarse-Grained Models for Aqueous Polyethylene Glycol Solutions. *J. Phys. Chem. B* **2014**, *118* (1), 323−329.

(11) Oelmeier, S. A.; Dismer, F.; Hubbuch, J. Molecular dynamics simulations on aqueous two-phase systems-Single PEG-molecules in solution. *BMC Biophys.* **2012**, *5* (1), 14.

(12) Prasitnok, K.; Wilson, M. R. A coarse-grained model for polyethylene glycol in bulk water and at a water/air interface. *Phys. Chem. Chem. Phys.* **2013**, *15* (40), 17093−17104.

(13) Marrink, S. J.; Risselada, H. J.; Yefimov, S.; Tieleman, D. P.; De Vries, A. H. The MARTINI force field: coarse grained model for biomolecular simulations. *J. Phys. Chem. B* **2007**, *111* (27), 7812−7824.

(14) Monticelli, L.; Kandasamy, S. K.; Periole, X.; Larson, R. G.; Tieleman, D. P.; Marrink, S. J. The MARTINI coarse-grained force field: extension to proteins. *J. Chem. Theory Comput.* **2008**, *4* (5), 819−834.

(15) Lee, H.; de Vries, A. H.; Marrink, S. J.; Pastor, R. W. A coarse-grained model for polyethylene oxide and polyethylene glycol: conformation and hydrodynamics. *J. Phys. Chem. B* **2009**, *113* (40), 13186−13194.

(16) Lee, H.; Pastor, R. W. Coarse-grained model for PEGylated lipids: effect of PEGylation on the size and shape of self-assembled structures. *J. Phys. Chem. B* **2011**, *115* (24), 7830−7837.

(17) Ghanbari, A.; Rahimi, M.; Dehghany, J. Influence of Surface Grafted Polymers on the Polymer Dynamics in a Silica−Polystyrene Nanocomposite: A Coarse-Grained Molecular Dynamics Investigation. *J. Phys. Chem. C* **2013**, *117* (47), 25069−25076.

(18) Corbierre, M. K.; Cameron, N. S.; Sutton, M.; Mochrie, S. G.; Lurio, L. B.; Rühm, A.; Lennox, R. B. Polymer-stabilized gold nanoparticles and their incorporation into polymer matrices. *J. Am. Chem. Soc.* **2001**, *123* (42), 10411−10412.

(19) Smith, J. S.; Bedrov, D.; Smith, G. D. A molecular dynamics simulation study of nanoparticle interactions in a model polymer-nanoparticle composite. *Compos. Sci. Technol.* **2003**, *63* (11), 1599−1605.

(20) Barbier, D.; Brown, D.; Grillet, A. C.; Neyertz, S. Interface between end-functionalized PEG oligomers and a silica nanoparticle studied by molecular dynamics simulations. *Macromolecules* **2004**, *37* (12), 4695−4710.

(21) Chevigny, C.; Dalmas, F.; Di Cola, E.; Gigmes, D.; Bertin, D.; Boué, F.; Jestin, J. Polymer-grafted-nanoparticles nanocomposites: Dispersion, grafted chain conformation, and rheological behavior. *Macromolecules* **2011**, *44* (1), 122−133.

(22) Wu, C. Simulated glass transition of poly(ethylene oxide) bulk and film: a comparative study. *J. Phys. Chem. B* **2011**, *115* (38), 11044−11052.

(23) Eliassi, A.; Modarress, H.; Mansoori, G. A. Densities of poly (ethylene glycol)+ water mixtures in the 298.15−328.15 K temperature range. *J. Chem. Eng. Data* **1998**, *43* (5), 719−721.

(24) Hong, B.; Panagiotopoulos, A. Z. Molecular dynamics simulations of silica nanoparticles grafted with poly (ethylene oxide) oligomer chains. *J. Phys. Chem. B* **2012**, *116* (8), 2385−2395.

(25) Song, B.; Yuan, H.; Jameson, C. J.; Murad, S. Role of surface ligands in nanoparticle permeation through a model membrane: a coarse-grained molecular dynamics simulations study. *Mol. Phys.* **2012**, *110* (18), 2181−2195.

(26) Karakoti, A. S.; Das, S.; Thevuthasan, S.; Seal, S. PEGylated inorganic nanoparticles. *Angew. Chem., Int. Ed.* **2011**, *50* (9), 1980−1994.

(27) Manson, J.; Kumar, D.; Meenan, B. J.; Dixon, D. Polyethylene glycol functionalized gold nanoparticles: the influence of capping density on stability in various media. *Gold Bull.* **2011**, *44* (2), 99−105.

(28) Rahme, K.; Chen, L.; Hobbs, R. G.; Morris, M. A.; O'Driscoll, C.; Holmes, J. D. PEGylated gold nanoparticles: polymer quantification as a function of PEG lengths and nanoparticle dimensions. *RSC Adv.* **2013**, *3* (17), 6085−6094.

(29) Li, Y.; Kröger, M.; Liu, W. K. Endocytosis of PEGylated nanoparticles accompanied by structural and free energy changes of the grafted polyethylene glycol. *Biomaterials* **2014**, *35* (30), 8467−8478.

(30) Nicholas, A. R.; Scott, M. J.; Kennedy, N. I.; Jones, M. N. Effect of grafted polyethylene glycol (PEG) on the size, encapsulation efficiency and permeability of vesicles. *Biochim. Biophys. Acta, Biomembr.* **2000**, *1463* (1), 167−178.

(31) Tirosh, O.; Barenholz, Y.; Katzhendler, J.; Priev, A. Hydration of polyethylene glycol-grafted liposomes. *Biophys. J.* **1998**, *74* (3), 1371−1379.

(32) Hattemer, G. D.; Arya, G. Viscoelastic Properties of Polymer-Grafted Nanoparticle Composites from Molecular Dynamics Simulations. *Macromolecules* **2015**, *48* (4), 1240−1255.

(33) Frischknecht, A. L. Forces between nanorods with end-adsorbed chains in a homopolymer melt. *J. Chem. Phys.* **2008**, *128* (22), 224902.

(34) Anne, A.; Demaille, C.; Moiroux, J. Terminal attachment of polyethylene glycol (PEG) chains to a gold electrode surface. Cyclic voltammetry applied to the quantitative characterization of the flexibility of the attached PEG chains and of their penetration by mobile PEG chains. *Macromolecules* **2002**, *35* (14), 5578−5586.

(35) Walkey, C. D.; Olsen, J. B.; Guo, H.; Emili, A.; Chan, W. C. Nanoparticle size and surface chemistry determine serum protein adsorption and macrophage uptake. *J. Am. Chem. Soc.* **2012**, *134* (4), 2139−2147.

DOI: 10.1021/acs.langmuir.6b01740
Langmuir 2016, 32, 7541−7555

(36) Oh, E.; Susumu, K.; Mäkinen, A. J.; Deschamps, J. R.; Huston, A. L.; Medintz, I. L. Colloidal stability of gold nanoparticles coated with multithiol-poly (ethylene glycol) ligands: importance of structural constraints of the sulfur anchoring groups. *J. Phys. Chem. C* **2013**, *117* (37), 18947−18956.
(37) Rissanen, S.; Kumorek, M.; Martinez-Seara, H.; Li, Y.-C.; Jamróz, D.; Bunker, A.; Nowakowska, M.; Vattulainen, I.; Kepczynski, M.; Róg, T. Effect of PEGylation on Drug Entry into Lipid Bilayer. *J. Phys. Chem. B* **2014**, *118* (1), 144−151.
(38) Magarkar, A.; Karakas, E.; Stepniewski, M.; Róg, T.; Bunker, A. Molecular dynamics simulation of PEGylated bilayer interacting with salt ions: a model of the liposome surface in the bloodstream. *J. Phys. Chem. B* **2012**, *116* (14), 4212−4219.
(39) Stepniewski, M.; Pasenkiewicz-Gierula, M.; Róg, T.; Danne, R.; Orlowski, A.; Karttunen, M.; Urtti, A.; Yliperttula, M.; Vuorimaa, E.; Bunker, A. Study of PEGylated lipid layers as a model for PEGylated liposome surfaces: Molecular dynamics simulation and langmuir monolayer studies. *Langmuir* **2011**, *27* (12), 7788−7798.
(40) Li, Y.-C.; Rissanen, S.; Stepniewski, M.; Cramariuc, O.; Róg, T.; Mirza, S.; Xhaard, H.; Wytrwal, M.; Kepczynski, M.; Bunker, A. Study of interaction between PEG carrier and three relevant drug molecules: piroxicam, Paclitaxel, and hematoporphyrin. *J. Phys. Chem. B* **2012**, *116* (24), 7334−7341.
(41) Song, B.; Yuan, H.; Jameson, C. J.; Murad, S. Permeation of nanocrystals across lipid membranes. *Mol. Phys.* **2011**, *109* (11), 1511−1526.
(42) Song, B.; Yuan, H.; Pham, S. V.; Jameson, C. J.; Murad, S. Nanoparticle permeation induces water penetration, ion transport, and lipid flip-flop. *Langmuir* **2012**, *28* (49), 16989−17000.
(43) Tanaka, M.; Sackmann, E. Polymer-supported membranes as models of the cell surface. *Nature* **2005**, *437* (7059), 656−663.
(44) Plimpton, S. Fast parallel algorithms for short-range molecular dynamics. *J. Comput. Phys.* **1995**, *117* (1), 1−19.
(45) Oroskar, P. A.; Jameson, C. J.; Murad, S. Surface-Functionalized Nanoparticle Permeation Triggers Lipid Displacement and Water and Ion Leakage. *Langmuir* **2015**, *31* (3), 1074−1085.
(46) Petros, R. A.; DeSimone, J. M. Strategies in the design of nanoparticles for therapeutic applications. *Nat. Rev. Drug Discovery* **2010**, *9* (8), 615−627.
(47) Wang, J.; Byrne, J. D.; Napier, M. E.; DeSimone, J. M. More effective nanomedicines through particle design. *Small* **2011**, *7* (14), 1919−1931.
(48) Bishop, C. C.; Powell, S.; Rutt, D.; Browse, N. L. Transcranial Doppler measurement of middle cerebral artery blood flow velocity: A validation study. *Stroke* **1986**, *17* (5), 913−915.
(49) Tieleman, D. P.; Marrink, S. J. Lipids out of equilibrium: Energetics of desorption and pore mediated flip-flop. *J. Am. Chem. Soc.* **2006**, *128* (38), 12462−12467.
(50) Bennett, W. D.; Tieleman, D. P. Water defect and pore formation in atomistic and coarse-grained lipid membranes: pushing the limits of coarse graining. *J. Chem. Theory Comput.* **2011**, *7* (9), 2981−2988.
(51) Lu, W.; Sun, Q.; Wan, J.; She, Z.; Jiang, X. G. Cationic albumin−conjugated pegylated nanoparticles allow gene delivery into brain tumors via intravenous administration. *Cancer Res.* **2006**, *66* (24), 11878−11887.
(52) Kim, H. R.; Gil, S.; Andrieux, K.; Nicolas, V.; Appel, M.; Chacun, H.; Desmaële, D.; Taran, F.; Georgin, D.; Couvreur, P. Low-density lipoprotein receptor-mediated endocytosis of PEGylated nanoparticles in rat brain endothelial cells. *Cell. Mol. Life Sci.* **2007**, *64* (3), 356−364.
(53) Daleke, D. L. Phospholipid flippases. *J. Biol. Chem.* **2007**, *282* (2), 821−825.
(54) Matsuzaki, K.; Murase, O.; Fujii, N.; Miyajima, K. An antimicrobial peptide, magainin 2, induced rapid flip-flop of phospholipids coupled with pore formation and peptide translocation. *Biochemistry* **1996**, *35* (35), 11361−11368.
(55) Devaux, P. F. Static and dynamic lipid asymmetry in cell membranes. *Biochemistry* **1991**, *30* (5), 1163−1173.
(56) Contreras, F. X.; Sánchez-Magraner, L.; Alonso, A.; Goñi, F. M. Transbilayer (flip-flop) lipid motion and lipid scrambling in membranes. *FEBS Lett.* **2010**, *584* (9), 1779−1786.
(57) Calvo, P.; Gouritin, B.; Chacun, H.; Desmaële, D.; D'Angelo, J.; Noel, J. P.; Georgin, D.; Fattal, E.; Andreux, J. P.; Couvreur, P. Long-circulating PEGylated polycyanoacrylate nanoparticles as new drug carrier for brain delivery. *Pharm. Res.* **2001**, *18* (8), 1157−1166.
(58) Brown, S. D.; Nativo, P.; Smith, J.-A.; Stirling, D. A.; Edwards, P. R.; Venugopal, B.; Flint, D. J.; Plumb, J. A.; Graham, D.; Wheate, N. J. Gold nanoparticles for the improved anticancer drug delivery of the active component of oxaliplatin. *J. Am. Chem. Soc.* **2010**, *132* (13), 4678−4684.
(59) Khavrutskii, I. V.; Gorfe, A. A.; Lu, B.; McCammon, J. A. Free energy for the permeation of Na+ and Cl− ions and their ion-pair through a zwitterionic dimyristoyl phosphatidylcholine lipid bilayer by umbrella integration with harmonic fourier beads. *J. Am. Chem. Soc.* **2009**, *131* (5), 1706−1716.

DOI: 10.1021/acs.langmuir.6b01740
Langmuir 2016, 32, 7541−7555